Journal of
Manufacturing and Materials Processing

MDPI

Article

SLA Resins Modification by Liquid Mixing with Ceramic Powders Aiming at Mechanical Property and Thermal Stability Enhancement for Rapid Tooling Applications

Anna Karatza [1,2,*], Panagiotis Zouboulis [1], Iakovos Gavalas [1], Dionisis Semitekolos [2], Artemis Kontiza [2], Melpo Karamitrou [2], Elias P. Koumoulos [3] and Costas Charitidis [2]

[1] BioG3D P.C., 1 Lavriou Str., Technological & Cultural Park of Lavrion, GR-19500 Lavrion, Greece
[2] RNANO Lab—Research Lab of Advanced, Composite, Nanomaterials & Nanotechnology, Department of Materials Science and Engineering, School of Chemical Engineering, National Technical University of Athens, Zographos, GR-15780 Athens, Greece
[3] IRES—Innovation in Research & Engineering Solutions, Rue Koningin Astridlaan 59B, 1780 Wemmel, Belgium
* Correspondence: akaratza@biog3d.gr

Abstract: Stereolithography (SL) additive manufacturing process provides increased dimensional precision, smooth surface finish and printing resolution range in the order of magnitude of 100 μm, allowing to obtain intricate 3D geometries. The incorporation of ceramic-based inclusions within liquid resins enhances the thermal and mechanical properties of the final 3D printed component while improving the surface finishing of the final parts; in this way, it expands the range of process applications and reduces the post-processing steps. The proposed approach investigates the bulk modification of commercial SLA resins mixed with ceramic powders of Al_2O_3 (grain size 1–10 μm) and SiO_2 (grain size 55–75 nm) aiming to improve 3D printed parts performance in terms of mechanical properties, dimensional stability and surface finishing compared with pure, unmodified resins. The produced materials were used for the development of inserts for injection moulding and were examined for their performance during the injection moulding process. The addition of particles in the nano- and micro-range is being employed to improve parts performance for rapid tooling applications whilst maintaining 3D printing accuracy, thermal and mechanical properties as well as achieving a smooth surface finishing compared with unmodified resins.

Keywords: ceramic resins; materials for additive manufacturing; injection moulding; resin formulations; 3D printing; stereolithography; photocurable resins; ceramic powders

Citation: Karatza, A.; Zouboulis, P.; Gavalas, I.; Semitekolos, D.; Kontiza, A.; Karamitrou, M.; Koumoulos, E. P.; Charitidis, C. SLA Resins Modification by Liquid Mixing with Ceramic Powders Aiming at Mechanical Property and Thermal Stability Enhancement for Rapid Tooling Applications. *J. Manuf. Mater. Process.* **2022**, *6*, 129. https://doi.org/10.3390/jmmp6060129

Academic Editors: Paolo Cicconi and Marco Mandolini

Received: 14 September 2022
Accepted: 17 October 2022
Published: 26 October 2022

1. Introduction

Ceramic materials have been at the centre of scientific research due to their wide range of applications and their unique physicochemical properties. Ceramics are known for their strength, hardness, thermal shock resistance, high chemical stability in harsh conditions and temperature performance [1–3]. Traditional practices (such as slip casting, injection moulding and dry pressing) used to shape and process ceramic parts are incapable of providing highly intricate 3D structures. The additive manufacturing process is paving the way to new routes towards the fabrication of highly complex 3D ceramic components [4–8].

In addition, the incorporation of inorganic additives such as silica and alumina particles in organic matrix reduces the thermal expansion coefficient while glass transition temperature and thermal stability of cured specimens are also improved [9]. Furthermore, investigations with various SLA-based resins showed a decrease in the coefficient of thermal expansion with increased ceramic content [10]. Disadvantages of ceramic additives

include the increment of the resin viscosity while the printing resolution is compromised due to internal light scattering [11]. Thus, the grain size and size distribution of the ceramic particles, the concentration of the ceramic powder and the homogeneity of the final solution must be optimised in order to tackle the aforementioned issues [12]. Several scientific reports demonstrated the use of SiO_2 [13,14] and Al_2O_3 [15,16] due to their excellent UV-absorption and high scattering coefficient [8,17].

However, in comparison with unmodified resins, the formulated hybrid ceramic resins experience increased internal scatterings due to the particle volume fraction that led to laser's penetration depth degradation [12]. The ceramic powder concentration within the resin matrix increases the shear-thinning behaviour of the formulated hybrid resins; therefore, by controlling ceramic powder concentration within the resin, the rheology of the final hybrid resin can be maintained or slightly altered, sustaining its processability. Thus, ceramic powder concentration compensation is required to maintain good processability. In this context, addition of ceramic particle loading was investigated, aiming to maintain SLA processability and part accuracy.

The utilised ceramic powders for AM process should satisfy the following requirements [7–9,18–22].

1. The refractive index (RI) of the ceramic powders has to present low variation from the one of the raw resins. Within UV spectrum range, Al_2O_3 and SiO_2 ceramic powders have an RI near 1.7 and 1.56, respectively, while the majority of the resin monomers show an RI near 1.5. For that reason, ceramic powders with low or medium RI are recommended, such as silica and alumina.
2. The median particle size of the ceramic powders should be smaller than the layer thickness, which lies between 25 and 100 μm. The smaller particle size improves the vertical resolution of the final 3D printed component. The optimum particle size is suggested to be around 0.05 μm and 10 μm.
3. The reduction of the particle size affects the specific surface area consequently. Smaller and finer particles generate a lot of internal scattering events. In contrast, the internal scattering is decreased when larger particles are used, and more light is transmitted. Less internal scattering events lead to large scattering length. Scattering length is defined as the free distance that a photon can travel before its direction changes again and becomes randomised. A ceramic slurry with a large scattering length is considered to have the same cured profile as the conventional, unmodified resin.

The scope of this study is to investigate the influence of small quantities of ceramic additives within SLA resins to produce hybrid ceramic resins aiming to improve the 3D printed parts performance in terms of surface finishing compared with unmodified resins, thermal and mechanical stability of the 3D printed components for high heat applications such as mould inserts for thermoplastic injection moulding, while retaining dimensional accuracy requirements of rapid tooling applications [6,20,23].

2. Materials and Methods

2.1. Formulation Development and 3D Printing Process

Commercial resins for SLA process have been utilised as matrix material. Here, the addition of 1 and 5% wt. ceramic particle loading was selected. The range of the lower and upper concentration limit was selected with a goal to avoid compromising the rheological properties of the formulated resins.

Two resin matrices were considered for the experimentation plan: (1) Formlabs High Temp resin (HT): a resin with high heat deflection temperature (HDT) of 238 °C @ 0.45 MPa, designed for fabrication of functional prototypes in high heat applications, such as hot gas and fluid routing; heat resistant mounts and housings; as well as fixtures, moulds and inserts. (2) Formlabs Surgical Guide resin (SG): a material used with the ability to produce parts with high dimensional accuracy and smooth surface finish; Formlabs Clear

resin (CL) was utilised as commonly used commercially available resin for benchmarking of dimensional accuracy study.

Considering the aforementioned requirements, 2 types of ceramic powders were selected for resin modification through liquid mixing: (1) Al_2O_3 micron powder (grain size 1–10 μm); (2) SiO_2 nanopowder (grain size 55–75 nm); all purchased from Nanografi.

The following methodology was utilised for the powder dispersion within selected resins and processing steps:

- The selected SLA system was Form 2 by Formlabs with a self-heating resin tank up to 35 °C a 405 nm near UV (violet) diode laser with 250 mW power and 140 μm laser spot size. Layer thickness ranges from 25 to 100 μm
- Resin–ceramic particles composition and liquid mixing process: the hybrid ceramic materials that were produced during this process were 1% and 5% *w*/*w* Al_2O_3 and 1% and 5% *w*/*w* SiO_2. For preprocessing of the powder a drying temperature of 110 °C was set, which is a few degrees above water boiling for 6–10 h to remove humidity residuals. Dispersion of ceramic powder within EtOH followed, using ultrasonic bath for 4 h and magnetic stirring for another 4 h for pre-mixing to ensure homogeneous dispersion and agglomeration reduction. Then, the EtOH-powder mixtures were poured within commercial selected resin followed by further ultrasonication and magnetic stirring. After mixing procedure, heating at a range of 40–60 °C is suggested for 1 h to remove EtOH.
- Printing process: Standard software-produced support structures were employed in order to ensure proper adhesion and scaffolding of the printed components to the build plate, taking into consideration the printing orientation. Support density values were set to 80% as per the slicer's suggestion and touchpoint sizes were adjusted marginally from 0.7 mm to 0.8 mm to enhance retention capability and avoid support breakage during fabrication due to potentially increased part density induced from addition of the powder to the resin. Layer heights of 50 μm were selected towards the optimum combination between printing time and printed part quality. Due to the selected printing equipment's restrictions, no alternative exposure times and laser scanning speeds could be investigated at this point.
- Post-processing: After 3D printing process, the fabricated specimens were treated with the material provider's suggested post-processing protocol. The 3D printed components were washed with isopropanol (IPA,99.8+% for analysis, from Acros-organics) for 6 min; supports removal was conducted followed by surface grinding to smoothly remove the support marks. Specimens were fully dried and photocured using FORM Cure at 80 °C for 120 min using 405 nm light source following the resin provider's recommendations.
- Thermal treatment: High Temp Resin requires further heat treatment to reach its optimal mechanical properties and high heat deflection temperature (HDT), as also recommended by Formlabs. Therefore, the specimens were heat-treated in an oven for 180 min at 160 °C.

2.2. Dimensional Tolerance, Shrinkage Evaluation Protocol and Weight Loss Assessment

Test artefacts were designed and fabricated (Figure 1) using each of the materials described above as a means of assessing dimensional accuracy of basic dimensions (width, height and thickness) of the printed parts, as well as defining suitable scale factors for size compensation while also considering shrinkage behaviour. During this step, several specimens were also prepared using the Formlabs Clear resin as a form of benchmarking against one of the most used commercial resins. Measurements of basic dimensions were acquired through stereo microscope inspection (Leica S9D) and averaged for a total number of 5 specimens. A handheld 3D scanner (Handyscan—Creaform) and VX elements software were implemented for the comparison of 3D printed parts with the nominal geometry. Weight loss assessment of the 3D printed components was also employed in two

stages, before and after thermal treatment. The evaluation of the mass difference was conducted using a triplet of specimens.

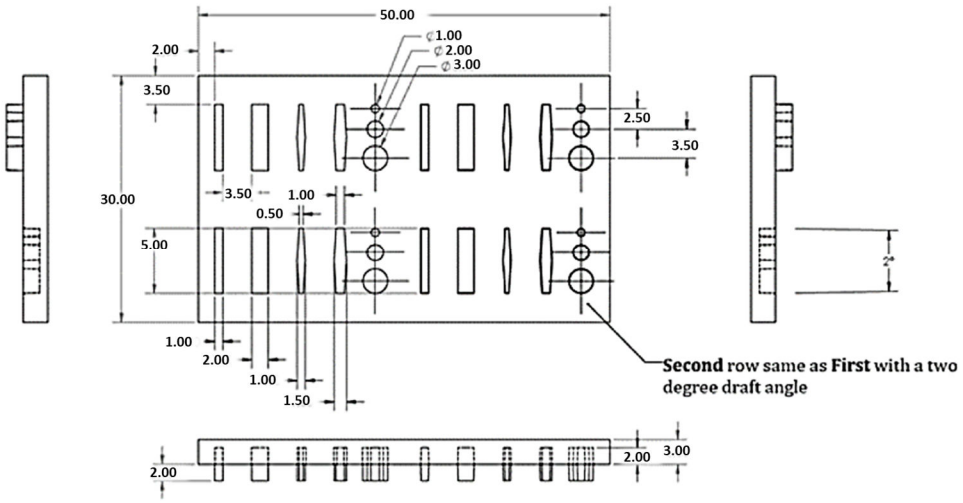

Figure 1. Design of selected test artefact for dimensional accuracy evaluation of the 3D printed parts.

2.3. Mechanical Testing

Flexural testing specimens following the ISO 178:2019 standard were 3D printed to compare the mechanical properties of the formulated materials with the original, non-reinforced HT resin and assess the impact of ceramic content type on material properties. Flexural strength was assessed by a 3-point bend test. The specimens built according to this standard were of rectangular shape and sized at 120 × 10 × 4 mm. The test introduced a bending load using a loading pin in the middle area of the piece while it was retained with 2 supporting pins spaced 60 mm apart. The samples were tested in a TE EDW-50/WDW-100 testing machine by JINAN. Five specimens were tested for each sample.

2.4. Surface Treatment and Adhesion Testing Protocol

In order to quantify the improvement in terms of material adhesion to the moulded polymer ABS, Magnum 3453 Natural by Trinseo as common feedstock material for injection moulding with regard to applied surface treatment, a set of circular coupons were prepared using the hybrid ceramic resin formulation. The disc-shaped specimens with a diameter of 25 mm and 1.5 mm thickness were inserted into the injection moulding machine cavities with matching dimensions to an Xplore micro-Injection moulder. An internal circular profile of 20 mm in diameter and 0.5 mm in depth was hollowed out from the centre of the insert with a 20° draft angle—a value selected to facilitate separation—focusing on flat surface adhesion, forming a cavity to be filled with injected ABS through a 6 mm runway (Figure 2). The injected ABS at 220 °C formed a circular concentration in the middle of the insert; the two parts were removed from the mould and heated at 70 °C. The holding pressure and time were controlled at 7 bar for 7 s, 9 bar for 0.1 s and 9 bar for 10 s. A Positest At-A Defelsko Ata20 adhesion tester was employed to measure the force required for the separation of the two components. The basic approach of gluing a test dolly to the coated surface and then exerting a perpendicular force to the surface in an effort to remove both the dolly and the coating from the substrate is common to all the international standards, such as ASTM D4541 and BS EN ISO 4624. A measure of the adhesion of the coating system is the force at which the coating fails, and the type of failure obtained. Trials have demonstrated that many aspects of the testing method, such as the mixing of the resin/glue, the preparation of the coating surface, the face of the dolly and the temperature of the test, all affect the results. The resin/glue was allowed to cure for 24 h and the dollies were pulled from the surface as shown in Figure 3. To reduce the risk of resin/glue

failures, the surface of the coating has been lightly abraded to promote adhesion of the adhesive to the surface. The equipment uses a 20 mm circular aluminium artefact and strong epoxy adhesive substance to exert pulling forces on a flat surface with a loading measuring capacity of up to 3500 psi. The device monitors the increasing pulling force up to the moment of separation, where the force measurement suddenly drops. In this case, the testing artefact was joined to the injected ABS (Figure 3).

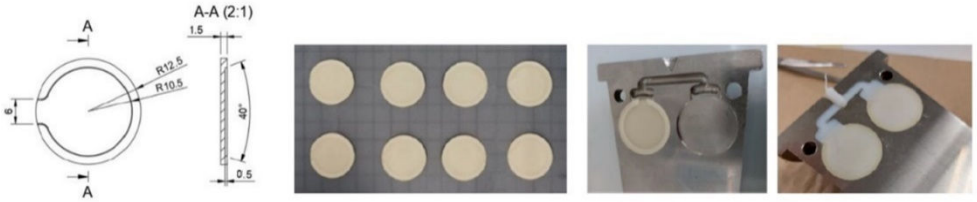

Figure 2. Circular inserts: design, fabricated parts, mould fitting and injection moulding trial.

Figure 3. Positest At-A Defelsko Ata20 Adhesion tester.

Four types of inserts with different surface treatment approaches were examined using this method:

- A set of untreated (as printed) coupons.
- A set of coupons that had undergone surface grinding. The coupons were procedurally processed by means of manual sanding, utilizing sandpaper with grit ranging from 120 to 2000. More specifically, dry sanding was employed up to 500 grits, whereas for higher grit values, wet sanding was appropriately applied.
- A set of sanded coupons, further dip coated with heated neat resin. The dip-coating process utilised neat resin heated up to 60 °C to decrease viscosity. The resin was placed in a borosilicate container and the coupons were submerged using a repurposed 3D printer motorised frame. This device was implemented into this process to ensure steady motion. The selected linear speed was set to 10 mm/min, the dwell time that the coupons spent in the liquid resin was set to 1 min and the retraction speed for the specimens to emerge from the resin was set to a lower value of 2 mm/min to avoid the formation of bubbles in the treated surface.
- A set of printed coupons with a commercial PTFE coating in spray form as a means to facilitate detachment during the trial. The PTFE was carefully applied indirectly using a cloth so as not to cause defects due to excess material droplets remaining on the surface of the part.

3. Results and Discussion

3.1. Dimensional Tolerances and Weight Loss Assessment

An initial comparative assessment of neat resins dimensional accuracy was conducted to select the matrix for hybrid ceramic formulation development. To preliminarily assess the geometrical fidelity of the 3D printed components to the nominal CAD values, rectangular torture test specimens (30 × 50 × 3 mm) were designed and fabricated. As per

the values of Table 1, the Surgical Guide resin appeared to achieve the highest dimensional accuracy, though the High Temp resin presented potential to reach the desired tolerances by implementing compensation scaling factors during printing process parametrisation. Ultimately, considering HT resin's properties and higher thermal deflection temperature values, HT was selected.

Table 1. Tolerance analysis for resin selection for hybrid material formulation development. HT: High Temperature, SG: Surgical Guide, CL: Clear by Formlabs.

	Height (Nominal Value: 30 mm)			**Width (Nominal Value: 50 mm)**			**Thickness (Nominal Value: 3 mm)**		
	HT	**SG**	**CL**	**HT**	**SG**	**CL**	**HT**	**SG**	**CL**
Mean Value average (mm)	30.14	29.97	30.06	49.94	50.04	49.82	2.98	3.01	2.98
Standard Deviation average (mm)	0.06	0.09	0.05	0.05	0.04	0.02	0.03	0.02	0.01
Standard error average (mm)	0.04	0.05	0.03	0.03	0.02	0.01	0.01	0.01	0.00
Dimension Upper Limit (mm)	**30.18**	**30.03**	**30.09**	**49.97**	**50.07**	**49.83**	**2.99**	**3.02**	**2.98**
Dimension Lower Limit (mm)	**30.11**	**29.92**	**30.04**	**49.91**	**50.02**	**49.81**	**2.97**	**3.01**	**2.97**

The selected matrix (HT resin) in combination with ceramic particle dispersions was also assessed in terms of dimensional accuracy of basic dimensions, as presented in Table 2. A comparative assessment was performed to preliminarily corroborate an increase in the dimensional accuracy of the basic dimensions of the fabricated artefacts attributed to the addition of the ceramic powder. Part orientation of printed components can affect the accuracy of the print, though in a per-case basis, depending on the individual features present on the printed parts. The selected orientation for the investigated specimens took into consideration their rectangular shape and aimed to minimize individual layer area values, which could potentially cause shape deformations due to shrinkage. The overall part dimensions across the three main axes—X, Y and Z—within the printer's cartesian space were measured in order to determine potential systematic errors and identify the need for compensation factors. Considering the nominal accuracy of the printer and the measured values (Tables 1 and 2), no compensation factors were required at this point and no alternative orientations were examined. As per the values in Table 2, the HT resin containing Al_2O_3 5% wt. presented the lowest deviation values from the nominal dimensions, while also exhibiting a smooth part finish.

Table 2. Tolerance analysis of basic dimensions of specimens fabricated with different hybrid ceramic formulations.

	HT	**HT Al_2O_3 1%**	**HT Al_2O_3 5%**	**HT SiO_2 1%**	**HT SiO_2 5%**
	Height (nominal value: 30 mm)				
Mean Value aver. (mm)	30.14	30.08	30.02	30.20	30.18
Standard Deviation aver. (mm)	0.06	0.03	0.04	0.08	0.04
Standard error aver. (mm)	0.04	0.02	0.02	0.05	0.03
Dimension Upper Limit (mm)	**30.18**	**30.10**	**30.04**	**30.25**	**30.20**
Dimension Lower Limit (mm)	**30.11**	**30.06**	**30.00**	**30.15**	**30.15**

	Width (nominal value: 50 mm)				
Mean Value aver. (mm)	49.94	49.99	49.99	49.92	49.92
Standard Deviation avg. (mm)	0.05	0.03	0.04	0.03	0.03
Standard error avg. (mm)	0.03	0.02	0.02	0.02	0.02
Dimension Upper Limit (mm)	**49.97**	**50.01**	**50.02**	**49.93**	**49.93**
Dimension Lower Limit (mm)	**49.91**	**49.97**	**49.97**	**49.90**	**49.90**
	Thickness (nominal value 3 mm)				
Mean Value avg. (mm)	2.98	3.00	3.01	3.04	3.06
Standard Deviation avg. (mm)	0.03	0.03	0.02	0.04	0.05
Standard error avg. (mm)	0.01	0.01	0.01	0.01	0.01
Dimension Upper Limit (mm)	**2.99**	**3.01**	**3.02**	**3.05**	**3.08**
Dimension Lower Limit (mm)	**2.97**	**2.99**	**3.01**	**3.03**	**3.05**

Further analysis regarding the dimensional integrity of the fine features embossed and debossed on the surface of the test artefacts was conducted to validate the results of the preliminary study, as well as to determine the existence of systematic errors in cases of more detailed geometries on printed parts. The numbering of the features and dimensions can be seen in Figure 4 below. Indicative images from the 3D printed specimens are presented in Figure 5. All measurements are presented in detail in Tables 3 and 4, while measurement analysis is subsequently reported in Tables A1 and A2 in Appendix A.

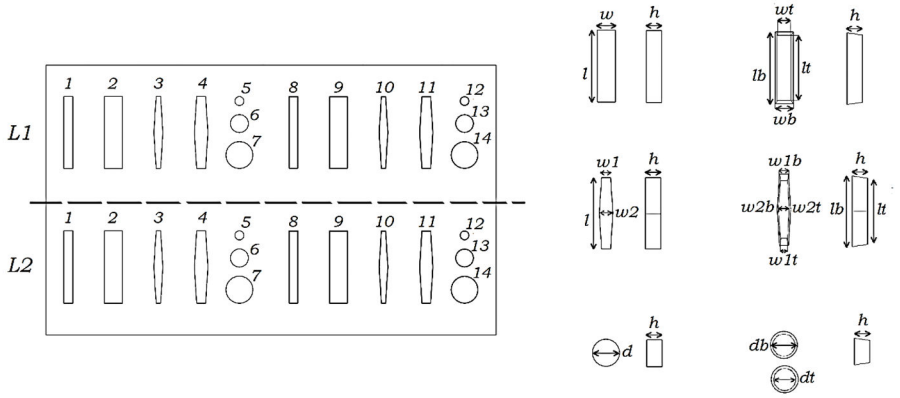

Figure 4. Feature numbering on test artefacts for measurement tabulation.

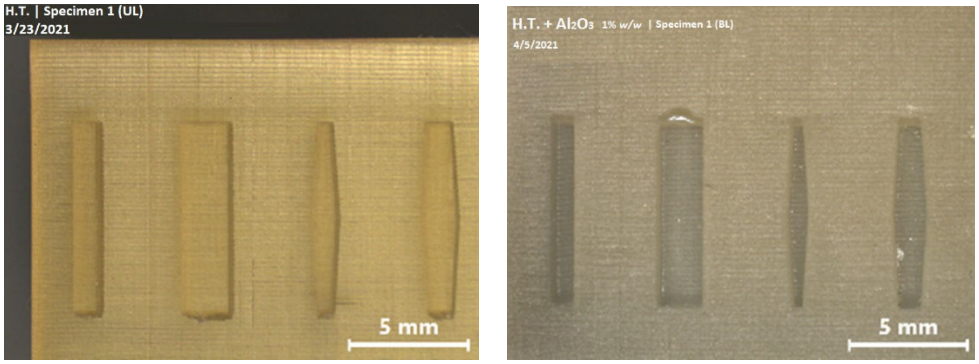

(**a**) (**b**)

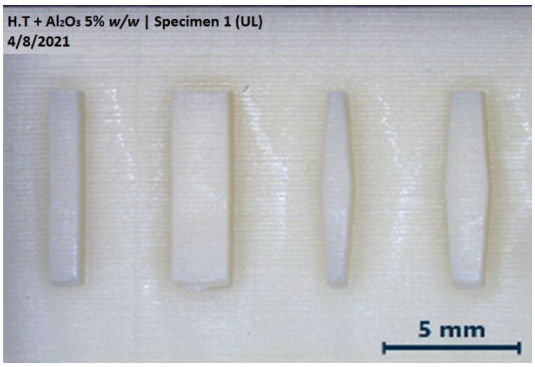

(**c**)

Figure 5. Indicative images of as-printed specimens for feature inspection using stereoscope imaging for measuring basic dimensions and tolerances for 30 × 50 × 3 mm nominal dimensions; (**a**)for pure resin (FormLabs High Temp—HT) prior to mixing with ceramic particles; (**b**) for resin with low content of ceramic particles (Al_2O_3); (**c**) for selected resin (FormLabs High Temp—HT) with increased content of ceramic particles (Al_2O_3).

Table 3. Measurement analysis for outward features.

	HT	HT + Al_2O_3 1%	HT + Al_2O_3 5%	HT +SiO_2 1%	HT +SiO_2 5%
Average error (mm)	−0.03	−0.01	0.02	−0.05	−0.05
Average deviation (mm)	0.09	0.04	0.02	0.14	0.15
Avg. error Z (mm)	−0.01	0.00	0.00	−0.01	0.00
Avg. error dev Z (mm)	0.01	0.00	0.00	0.00	0.01
Avg. error XY (mm)	−0.02	−0.01	−0.01	−0.03	−0.03
Avg. error dev XY (mm)	0.08	0.04	0.04	0.13	0.13

Table 4. Measurement analysis for inward features.

	HT	HT + Al_2O_3 1%	HT + Al_2O_3 5%	HT +SiO_2 1%	HT +SiO_2 5%
Average error (mm)	0.13	0.13	0.11	0.12	0.10
Average deviation (mm)	0.10	0.10	0.15	0.09	0.08
Avg. error Z (mm)	0.03	0.03	0.03	0.02	0.02
Avg. error dev Z (mm)	0.01	0.02	0.02	0.01	0.01
Avg. error XY (mm)	0.13	0.17	0.14	0.11	0.10
Avg. error dev XY (mm)	0.10	0.13	0.10	0.09	0.08

As per the abovementioned results, it is evident that hybrid formulations containing Al_2O_3 present the most stable printing results with dimensions either within, or very close to the required limits of ±0.020 mm. Outward features appear to possess highly accurate materialisation, imprinting even the finest features with satisfactory dimensional integrity, whereas inward features require the application of compensation factors over horizontal dimensions in the order of 10–15% to reach the desired values (Figure 6). The particle size of ceramic powders influence homogeneity and dispersion in the resin matrix and also determine the scattering level. Therefore, comparing the two different ceramic powders in 5% concentration to the resin matrix, the Al_2O_3 powder with higher particle dimension within the range of 1–10 μm suppresses unwanted excess of scattering effects compared with the SiO_2 nanosized particle powder, which promotes aggregation occurrence and higher uncontrollable scattering levels that downgrade the printing accuracy.

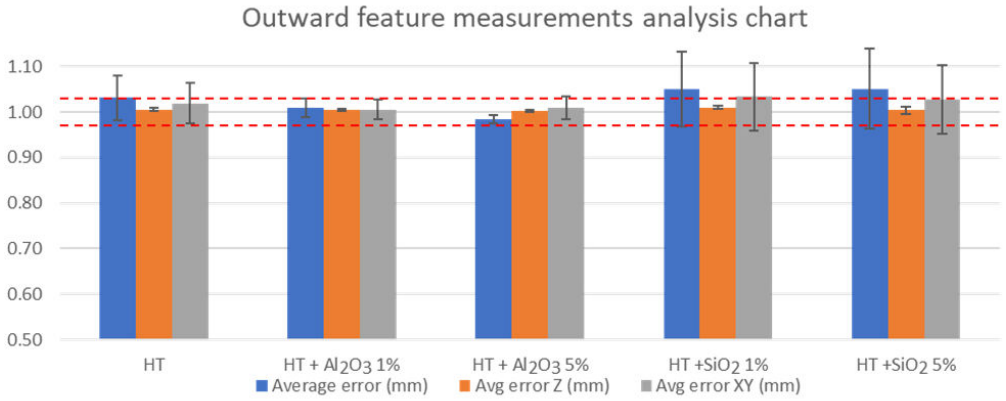

(**a**)

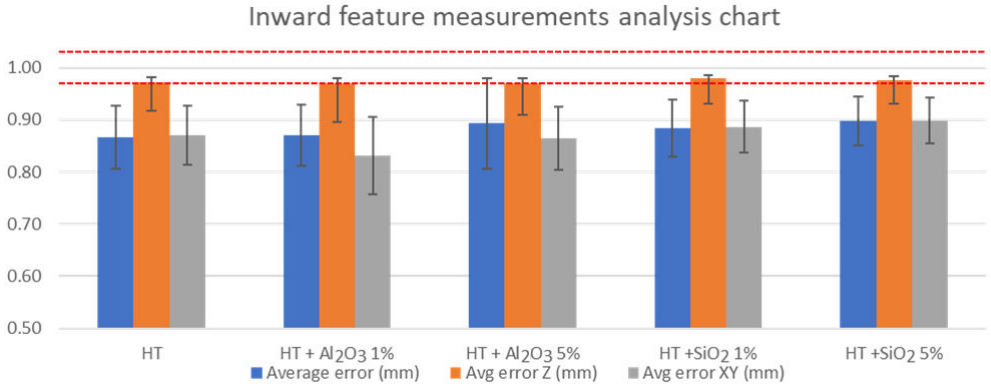

(**b**)

Figure 6. Feature measurements analysis and compliance with tolerance requirements charts. (**a**) Outwrads feature measurements; (**b**) Inward feature measurements analysis charts.

The addition of 5% Al_2O_3 powder results in light scattering phenomena and maximisation of curing width. Therefore, powder particles prevent the formation of the "staircase" effect alongside the fabrication orientation, resulting in non-visible layer lines along the printing direction and smooth surface finishing, as depicted in Figure 7.

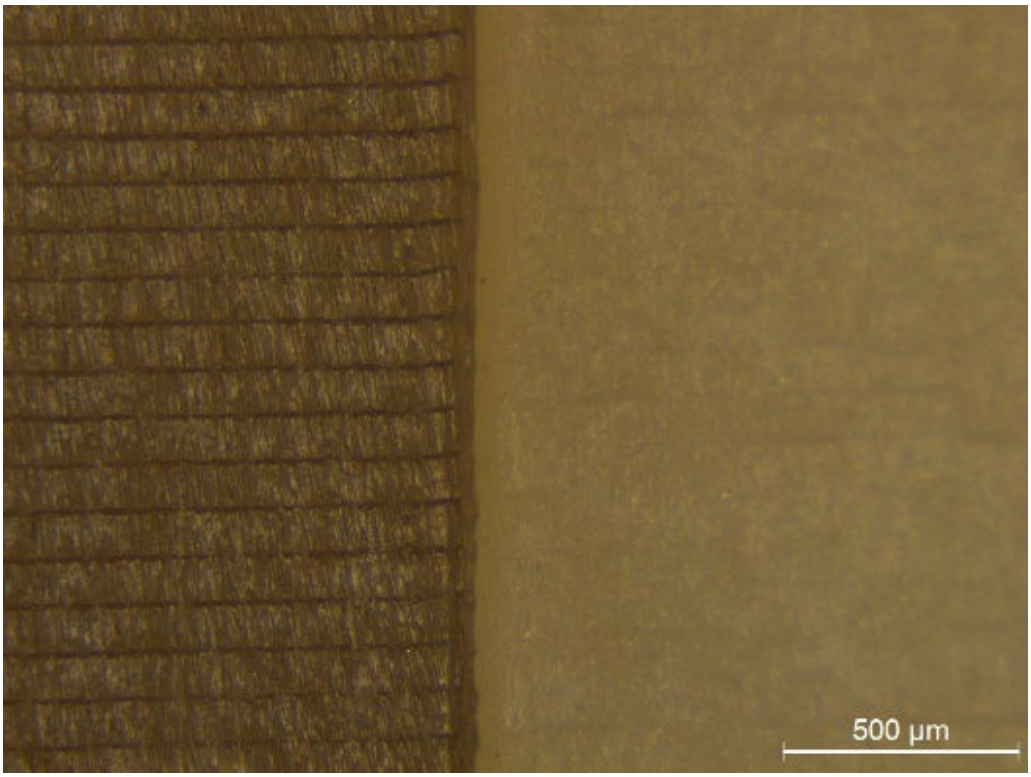

Figure 7. Stereomicroscopy image of two 3D printed specimens using raw HT resin (**left**) and hybrid ceramic HT resin (**right**). The printing layers of raw HT resin are evident along the printing axis while they are concealed in the hybrid ceramic**.**

With regard to the effect of the inclusion of the ceramic additives on orthogonal shapes, evaluation of 3D printed components consisting mainly of prismatic shapes was carried out using 3D scanning and appropriate geometry inspection software. The specimens were fabricated using 5% Al_2O_3 HT resin as the formulation appeared to present the most favourable properties in terms of printing accuracy and surface quality. In sample measurements taken on nominal 90° angles, the measured values and the observed deviations were kept within a 0.5° range (Figure 8), indicating no detrimental effect from the ceramic addition to the resin.

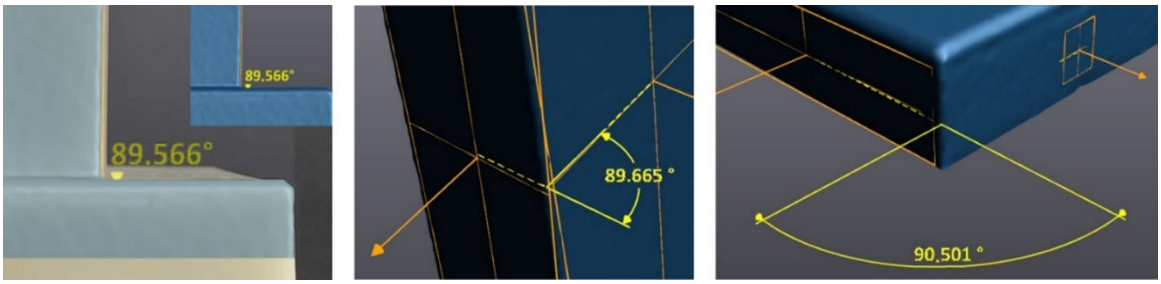

Figure 8. Assessment of the orthogonality preservation between the printed and scanned model.

The specimens were evaluated also for their weight loss before and after thermal treatment at 160 °C for 3 h in air atmosphere. Under thermal treatment, a small amount of weight loss was recorded indicating the removal of humidity and polymeric binders (Figure 9). Evaluation of the weight loss was performed in triplicate. The mean mass of the specimens before thermal treatment was 5.6239 g with a standard deviation of C0.0106 g, while the treated specimens had a lower mass of 5.6085 g with a standard deviation of 0.0109 g.

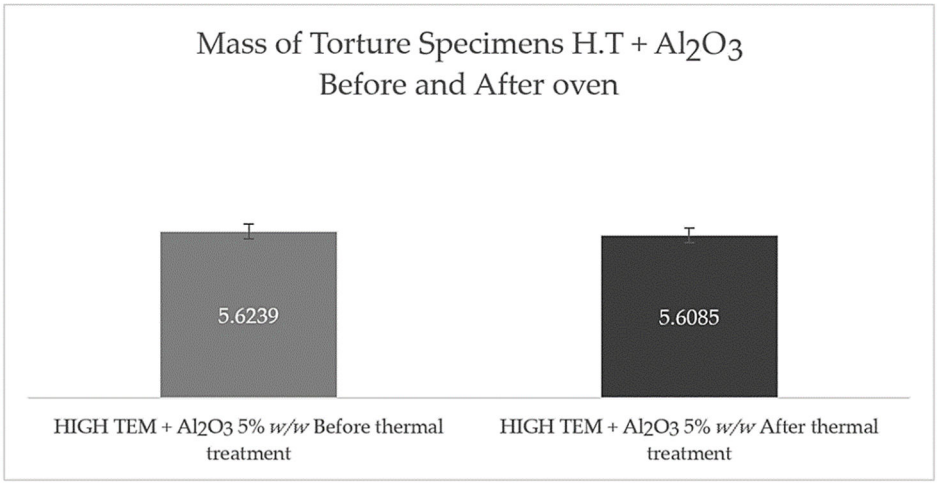

Figure 9. Weight loss assessment of the formulated hybrid ceramic resin, before and after thermal treatment.

3.2. Mechanical Properties Results

The flexural strength, strain at max stress (%) and flexural modulus are demonstrated in Table 5. The two ceramic powders exhibit different effects on the mechanical properties of the resin. More specifically, for the Al_2O_3 powder, increased concentration leads to higher flexural strength (+13.5% increase for 5% powder), while on the SiO_2, lower concentration leads to better mechanical behaviour (+18% increase for 1% powder). On the contrary, 1% addition of Al_2O_3 does not seem to have a major impact on the resin's properties (−9.1%; within the error limits), while resin with 5% SiO_2 exhibits dwindled flexural strength of 17% (Figure 10). The same pattern is also observed for the flexural strain at max stress, where resin with 5% Al_2O_3 and 1% SiO_2 exhibit longer elongation at break, a similar value for the resin with 1% Al_2O_3 and decrease for the 5% SiO_2 (Table 5). These results also justify the values of flexural modulus since it is the ratio of stress to strain during the flexural deformation or bending.

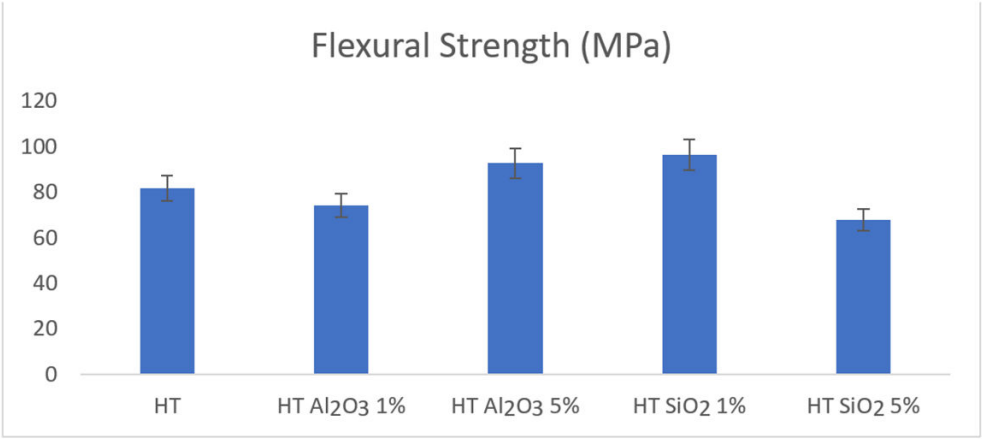

Figure 10. Flexure tests of the fabricated specimens for mechanical properties assessment. The dotted line corresponds to the Flexure Modulus Mean Value (MPa), while the orange bars denote the percentage difference from the Formlabs Standard High Temp resin.

Table 5. Flexural test results.

	Maximum Stress (MPa)	Flexural Strain at Max Stress (%)	Flexural Modulus (GPa)
HT	81.59 ± 22.86	4.95%	2.74 ± 0.16
HT Al_2O_3 1%	74.16 ± 11.15	4.95%	2.50 ± 0.05
HT Al_2O_3 5%	92.58 ± 12.00	5.56%	2.69 ± 0.12
HT SiO_2 1%	96.27 ± 13.58	5.47%	2.81 ± 0.16
HT SiO_2 5%	67.62 ± 20.68	4.24%	2.81 ± 0.23

3.3. Adhesion Testing in Different Surface Treatment Approaches

According to the results below, surface treatments decreased adhesion by 47%. Dip coating of the coupons did not exhibit a significant alteration in the adhesion of the coupons compared with only sanded parts. PTFE-coated inserts exhibited no bonding at all, making the quantified investigation unable to provide a numerical value (Table 6).

Table 6. Adhesion test quantitative results.

Coupon	Specimens No	Separation Pressure (MPa)	Separation Force (N)
As-printed	1	0.255	8.01
	2	0.262	8.23
Sanded	1	0.131	4.11
	2	0.131	4.11
Sanded + Dip-coated	1	0.131	4.11
	2	0.145	4.55
As-printed with PTFE spray	1	0	0
	2	0	0

4. Conclusions

During this study, two commercial SLA resins HT and SG were used along with two different ceramic powders (SiO_2 and Al_2O_3), in order to fabricate a hybrid ceramic resin for rapid tooling applications. Regarding the dimensional accuracy assessment, the SG resin appeared to achieve the highest dimensional accuracy, though the HT resin presented potential to reach the desired tolerances by implementing compensation scaling factors during printing process parametrisation.

Ultimately, considering HT resin's properties and higher thermal deflection temperature values, HT was selected. A comparative assessment was performed to preliminarily corroborate an increase in the dimensional accuracy of the basic dimensions of the fabricated artefacts attributed to the addition of the ceramic powder while also presenting an optimised surface finishing compared with the HT resin without ceramic inclusions. The HT resin was selected as the preferable resin matrix based on the initial comparative assessment of the pure resins that did not present excessive difference from the other matrices; however, the selected HT presents high heat deflection temperature that is preferable for rapid tooling applications. The HT Al_2O_3 5% was selected as optimum to perform further testing since it presents the lowest standard deviation average compared with the other hybrid–resin formulations from the analysis of external dimensions of the artefacts tests (Table 3) and the feature measurement analysis combined with the mechanical properties of the different compositions. Specifically, Al_2O_3 5% presents the best performance in the outward features, while in inward feature measurements the SiO_2 outperform the Al_2O_3 5% in dimensional accuracy. Mechanical properties are highly considerable for rapid tooling application; therefore, the HT Al_2O_3 5% was finally selected to perform adhesion tests, as the main objective was the investigation of post-process alternatives to

further improve surface treatment of the selected hybrid–resin. Samples of Al_2O_3 5% were able to sustain more stress before brakeage.

Rapid tooling applications require increased dimensional accuracy and adequate surface finishing along with high deflection temperature and increased mechanical properties. The addition of 5% Al_2O_3 in HT resin sustains the dimensional accuracy of the parts while presenting improved surface finish by consoling the layer lines alongside the 3D printed direction without affecting the mechanical performance of the 3D printed parts.

HT resin containing Al_2O_3 5% wt. presented the lowest deviation values from the nominal dimensions, while also exhibiting a smooth part finish. Hybrid formulations containing Al_2O_3 present the most stable printing results with dimensions either within, or very close to, the required limits of ±0.02 mm. Outward features appear to possess highly accurate materialisation, imprinting even the finest features with satisfactory dimensional integrity, whereas inward features require the application of compensation factors over horizontal dimensions of the order of 10–15% in order to reach the desired values. Thus, 5% of AL_2O_3 resin formulation is considered to be a suitable alternative to pure resin, being able to substitute the original material without hindering its overall mechanical properties. As part of the adhesion testing, surface treatments decreased adhesion by 47%. Dip coating of the coupons did not exhibit a significant alteration in the adhesion of the coupons compared with only sanded parts. PTFE-coated inserts exhibited no bonding at all, making the quantified investigation unable to provide a numerical value.

As a result, from the above, the hybrid ceramic resin HT + Al_2O_3 5% wt. was considered to be the optimum formulation for the production of 3D printed ceramic parts for the rapid tooling process exhibiting sufficient mechanical, thermal and fidelity properties. Further investigation of the rheological properties needs to be performed for further formulation and process optimisation. Further evaluation of mechanical performance of final insert designs during operational conditions in injection moulding production trials will be carried out, and the possibility to introduce toughening agents in selected material formulation will be considered, if required.

Author Contributions: Conceptualization, A.K. (Anna Karatza) and E.P.K.; Funding acquisition, A.K. (Anna Karatza), E.P.K. and C.C.; Methodology, A.K. (Anna Karatza), P.Z. and I.G.; Project administration, C.C., E.P.K. and A.K. (Anna Karatza); Investigation, I.G., P.Z., D.S., M.K. and A.K. (Artemis Kontiza); Writing—review and editing, A.K. (Anna Karatza), P.Z. and I.G. All authors have read and agreed to the published version of the manuscript.

Funding: This research was funded by European research project imPURE, grant number 101016262.

Data Availability Statement: Data available upon request

Conflicts of Interest: The authors declare no conflict of interest.

Appendix A

Table A1. Dimensional analysis detailed measurement results (outward features).

L1	Nominal Value (mm)	HT			HT + Al_2O_3 1%			HT + Al_2O_3 5%			HT + SiO_2 1%			HT +SiO_2 5%		
		1	2	3	1	2	3	1	2	3	1	2	3	1	2	3
1.l	8.00	8.06	8.08	8.10	8.07	8.06	8.02	8.04	8.04	8.01	8.12	8.15	8.14	8.09	8.10	8.08
1.w	1.00	1.04	1.05	1.04	1.02	1.03	1.02	1.02	1.02	1.02	1.08	1.07	1.10	1.11	1.09	1.09
1.h	2.00	1.91	1.92	1.91	1.90	1.94	1.91	2.02	1.94	1.94	1.96	1.89	1.92	1.86	1.79	1.86
2.l	8.00	8.09	8.08	8.07	8.05	8.06	8.04	8.06	8.01	8.03	8.14	8.09	8.10	8.12	8.09	8.11
2.w	2.00	2.03	2.05	2.02	2.00	2.01	2.03	2.03	2.01	2.06	2.05	2.03	2.01	2.07	2.07	2.06
2.h	2.00	1.90	1.91	1.92	2.02	1.97	1.96	1.97	1.98	1.93	1.82	1.85	1.86	1.82	1.83	1.85

3.l	8.00	8.06	8.10	8.07	8.04	8.01	8.05	8.10	8.02	8.06	8.11	8.10	8.12	8.11	8.08	8.10
3.w1	0.50	0.61	0.60	0.64	0.55	0.56	0.58	0.56	0.56	0.59	0.70	0.69	0.68	0.65	0.65	0.66
3.w2	1.00	1.03	1.05	1.06	1.01	1.03	1.04	1.01	1.03	1.04	1.08	1.05	1.06	1.07	1.06	1.05
3.h	2.00	1.92	1.88	1.91	1.92	1.90	1.92	2.00	1.93	1.95	1.92	1.87	1.88	1.80	1.85	1.82
4.l	8.00	8.06	8.08	8.06	8.06	8.06	8.07	8.07	8.01	8.05	8.15	8.14	8.08	8.09	8.11	8.09
4.w1	1.00	1.08	1.08	1.10	1.02	1.00	1.05	1.07	1.09	1.06	1.15	1.10	1.12	1.11	1.10	1.10
4.w2	1.50	1.52	1.54	1.53	1.53	1.55	1.54	1.51	1.54	1.52	1.55	1.50	1.53	1.57	1.54	1.54
4.h	2.00	1.92	1.90	1.92	1.97	1.93	1.99	1.99	1.95	1.95	1.89	1.86	1.91	1.79	1.85	1.86
5.d	1.00	1.04	1.08	1.06	1.02	1.03	1.02	1.03	1.02	1.01	-	-	-	1.10	1.16	1.13
5.h	2.00	1.89	1.87	1.85	1.90	1.89	1.94	2.01	1.93	1.95				1.88	1.43	1.87
6.d	2.00	2.13	2.11	2.11	2.02	2.01	2.03	2.04	2.02	2.02	2.05	2.03	3.03	2.06	2.09	2.03
6.h	2.00	1.94	1.92	1.94	1.90	1.89	1.94	2.01	1.94	1.95	1.92	1.91	1.93	1.89	1.86	1.86
7.d	3.00	3.03	3.05	3.05	3.00	3.03	3.02	3.01	3.03	3.03	3.05	3.04	3.07	3.03	3.05	3.04
7.h	2.00	1.93	1.90	1.89	1.90	1.89	1.94	2.01	1.93	1.95	1.92	1.91	1.92	1.82	1.85	1.87
8.lb	8.00	8.08	8.09	8.05	8.06	8.02	8.04	8.06	8.02	8.05	8.11	8.09	8.12	8.08	-	8.08
8.lt	7.93	7.93	7.91	7.94	7.98	7.91	7.98	7.94	7.93	7.96	7.95	7.99	7.96	7.80	-	7.88
8.wb	1.00	1.08	1.06	1.04	1.01	1.03	1.03	1.01	1.04	1.03	1.10	1.12	1.07	1.10	-	1.10
8.wt	0.93	0.96	0.93	0.96	0.94	0.96	0.94	0.96	0.95	0.94	0.94	0.94	0.95	0.94	-	0.95
8.h	2.00	1.91	1.89	1.89	1.96	1.96	1.96	1.93	1.94	1.95	1.82	1.79	1.83	1.79	-	1.82
9.lb	8.00	8.10	8.09	8.07	8.03	8.06	8.04	8.07	8.06	8.05	8.10	8.09	8.11	8.09	8.11	8.12
9.lt	7.93	7.91	7.94	7.92	7.94	7.93	7.92	7.93	7.91	7.97	7.94	7.93	7.96	7.93	7.90	7.90
9.wb	2.00	2.06	2.08	2.06	2.05	2.03	2.04	2.06	2.06	2.02	2.03	2.04	2.03	2.04	2.17	2.14
9.wt	1.93	1.94	1.95	1.97	1.95	1.96	1.94	1.96	1.95	1.93	1.96	1.91	1.95	1.91	1.98	1.95
9.h	2.00	1.88	1.88	1.88	2.00	1.99	1.97	1.92	1.98	1.93	1.82	1.82	1.80	1.82	1.84	1.86
10.lb	8.00	8.10	8.07	8.06	8.09	8.10	8.06	8.06	8.02	8.06	8.12	-	8.08	8.08	8.10	8.10
10.lt	7.93	7.87	7.88	7.88	7.94	7.93	7.97	7.84	7.80	7.95	7.96	-	7.98	7.33	7.86	7.90
10.w1b	0.50	0.62	0.62	0.61	0.56	0.54	0.58	0.58	0.58	0.58	0.70	-	0.70	0.74	0.71	0.69
10.w1t	0.43	0.56	0.55	0.56	0.47	0.45	0.47	0.48	0.51	0.43	0.63	-	0.65	0.68	0.67	0.59
10.w2b	1.00	1.02	1.05	1.06	1.01	1.01	1.02	1.00	1.01	0.98	1.08	-	1.07	1.07	1.08	1.08
10.w2t	0.93	0.92	0.94	0.93	0.90	0.90	0.90	0.94	0.94	0.94	0.94	-	0.94	0.92	0.95	0.94
10.h	2.00	1.93	1.93	1.91	1.99	1.92	1.97	1.94	1.96	1.90	1.87	-	1.87	1.85	1.85	1.87
11.lb	8.00	8.03	8.05	8.07	8.06	8.01	8.05	8.08	8.02	8.05	8.09	8.06	8.08	8.06	8.03	8.05
11.lt	7.93	7.97	7.97	7.94	7.94	7.95	7.93	7.96	7.90	7.96	7.98	8.01	7.97	8.01	7.94	7.96
11.w1b	1.00	1.05	1.05	1.05	1.01	1.03	1.04	1.06	1.07	1.01	1.10	1.10	1.05	1.10	1.12	1.09
11.w1t	0.93	1.00	1.00	0.97	0.90	0.92	0.94	0.97	0.95	0.97	0.97	1.06	0.96	1.06	0.99	1.02
11.w2b	1.50	1.53	1.52	1.53	1.51	1.54	1.51	1.49	1.50	1.52	1.51	1.52	1.55	1.52	1.51	1.50
11.w2t	1.43	1.46	1.47	1.43	1.46	1.46	1.48	1.45	1.43	1.44	1.45	1.43	1.45	1.43	1.45	1.46
11.h	2.00	1.92	1.92	1.91	1.99	1.91	1.89	1.92	1.92	1.97	1.90	1.85	1.88	1.85	1.83	1.86
12.db	1.00	1.03	1.04	1.05	1.03	1.03	1.02	1.01	1.00	0.99	-	1.08	-	-	1.08	-
12.dt	0.93	0.90	0.94	0.94	0.93	0.94	0.94	0.91	0.92	0.90	-	0.90	-	-	0.90	-
12.h	2.00	1.95	1.94	1.92	1.96	1.93	1.96	1.92	1.97	1.94	-	1.86	-	-	1.86	-
13.db	2.00	2.03	2.02	2.01	2.00	2.00	2.01	2.00	2.02	1.99	2.06	2.09	2.07	2.06	2.04	2.04
13.dt	1.93	1.96	1.93	1.95	1.92	1.95	1.91	1.93	1.93	1.92	1.93	1.93	1.95	1.95	1.97	1.97
13.h	2.00	1.91	1.91	1.93	1.96	1.93	1.96	1.92	1.97	1.94	1.91	1.88	1.86	1.83	1.87	1.87
14.db	3.00	3.01	3.03	3.00	3.02	3.01	3.02	3.01	3.01	3.00	3.03	3.05	3.04	3.05	3.00	3.00
14.dt	2.93	2.96	2.92	2.96	2.94	2.94	2.95	2.93	2.95	2.93	2.96	2.94	2.96	2.93	2.90	2.90
14.h	2.00	1.91	1.92	1.89	1.96	1.93	1.96	1.92	1.96	1.94	1.91	1.88	1.87	1.85	1.87	1.87

Table A2. Dimensional analysis detailed measurement results (inward features).

L2	Nominal Value (mm)		HT			HT + Al_2O_3 1%			HT + Al_2O_3 5%			HT +SiO_2 1%			HT +SiO_2 5%			
			1	2	3	1	2	3	1	2	3	1	2	3	1		2	3
1.l	8.00		7.66	7.78	7.80	7.67	7.66	7.62	7.74	7.68	7.71	7.72	7.85	7.84	7.69		7.70	7.68
1.w	1.00	0.74	0.85	0.74	0.82	0.83	0.82	0.84	0.79	0.85	0.78		0.77		0.75	0.81	0.79	0.79
2.l	8.00	7.76	7.78	7.70	7.67	7.66	7.62	7.74	7.74	7.71	7.82		7.85		7.74	7.79	7.80	7.78
2.w	2.00	1.73	1.75	1.62	1.60	1.67	1.63	1.63	1.61	1.66	1.75		1.73		1.61	1.77	1.77	1.76
2.h	2.00	2.00	2.01	1.99	1.99	1.99	2.01	1.99	2.01	2.01	2.01		2.00		2.01	1.99	2.00	2.01
3.l	8.00	7.66	7.68	7.80	7.67	7.66	7.62	7.74	7.68	7.71	7.82		7.75		7.74	7.79	7.70	7.78
3.w1	0.50	0.00	0.00	0.00	0.00	0.00	0.00	0.00	0.00	0.00	0.00		0.00		0.00	0.00	0.00	0.00
3.w2	1.00	0.84	0.75	0.74	0.82	0.83	0.82	0.72	0.72	0.75	0.88		0.87		0.90	0.81	0.89	0.89
4.l	8.00	7.76	7.68	7.70	7.77	7.76	7.72	7.68	7.74	7.71	7.82		7.85		7.84	7.69	7.80	7.68
4.w1	1.00	0.74	0.75	0.84	0.82	0.83	0.82	0.77	0.77	0.82	0.88		0.87		0.80	0.81	0.79	0.89
4.w2	1.50	1.22	1.14	1.13	1.23	1.25	1.28	1.21	1.24	1.22	1.25		1.20		1.13	1.17	1.24	1.24
4.h	2.00	2.00	2.01	1.99	1.99	1.99	2.01	1.99	2.01	2.01	2.01		2.00		2.01	1.99	2.00	2.01
7.d	3.00	2.73	2.65	2.65	2.70	2.73	2.62	2.71	2.73	2.73	2.75		2.64		2.77	2.63	2.65	2.74
7.h	2.00	2.01	1.99	2.00	1.99	0.84	0.65	2.01	1.99	2.01	2.00		2.00		2.01	2.00	2.00	1.99
8.lb	8.00	7.76	7.78	7.80	7.77	7.76	7.72	7.74	7.74	7.68	7.72		7.75		7.84	7.79	7.80	7.68
8.wb	1.00	0.84	0.85	0.74	0.82	0.78	0.79	0.72	0.72	0.72	0.88		0.87		0.80	0.91	0.89	0.79
9.lb	8.00	7.76	7.68	7.70	7.67	7.66	7.72	7.74	7.74	7.71	7.82		7.85		7.74	7.79	7.80	7.68
9.wb	2.00	1.63	1.75	1.72	1.70	1.71	1.63	1.73	1.71	1.66	1.75		1.63		1.61	1.77	1.77	1.76
9.h	2.00	1.99	2.00	2.00	2.00	2.01	2.00	1.99	1.99	1.99	2.00		1.99		1.99	1.99	2.01	1.99
10.lb	8.00	7.66	7.68	7.80	7.67	7.76	7.62	7.74	7.64	7.61	7.72		7.85		7.84	7.79	7.70	7.78
10.w1b	0.50	0.00	0.00	0.00	0.00	0.00	0.00	0.00	0.00	0.00	0.00		0.00		0.00	0.00	0.00	0.00
10.w1t	0.43	0.00	0.00	0.00	0.00	0.00	0.00	0.00	0.00	0.00	0.00		0.00		0.00	0.00	0.00	0.00
10.w2b	1.00	0.74	0.85	0.74	0.82	0.73	0.82	0.72	0.82	0.82	0.78		0.87		0.80	0.81	0.89	0.89
11.lb	8.00	7.66	7.78	7.70	7.77	7.76	7.72	7.74	7.74	7.61	7.82		7.85		7.84	7.79	7.80	7.78
11.w1b	1.00	0.74	0.75	0.84	0.82	0.73	0.72	0.72	0.82	0.72	0.78		0.77		0.80	0.91	0.79	0.89
11.w2b	1.50	1.12	1.14	1.23	1.23	1.25	1.24	1.21	1.14	1.12	1.25		1.20		1.23	1.17	1.24	1.14
11.h	2.00	1.99	2.01	2.00	2.00	1.99	2.00	2.01	1.99	2.00	2.00		1.99		1.99	1.99	2.01	2.00
12.db	1.00	0.84	0.85	0.74	0.72	0.83	0.82	0.82	0.72	0.82	0.78		0.77		0.90	0.81	0.79	0.89
14.db	3.00	2.63	2.65	2.75	2.60	2.63	2.72	2.71	2.63	2.63	2.65		2.64		2.67	2.73	2.75	2.74
14.h	2.00	1.99	1.99	2.01	1.99	0.50	0.61	2.00	1.99	2.00	2.01		2.00		2.00	2.00	1.99	1.99

References

1. He, R.; Liu, W.; Wu, Z.; An, D.; Huang, M.; Wu, H.; Jiang, Q.; Ji, X.; Wu, S.; Xie, Z. Fabrication of complex-shaped zirconia ceramic parts via a DLP- stereolithography-based 3D printing method. *Ceram. Int.* **2018**, *44*, 3412–3416.
2. Janssen, R.; Scheppokat, S.; Claussen, N. Tailor-made ceramic-based componentsadvantages. *Eur. Ceram. Soc.* **2018**, *28*, 1369–1379.
3. Xing, H.; Zou, B.; Wang, X.; Hu, Y.; Huang, C.; Xue, K. Fabrication and characterization of SiC whiskers toughened Al_2O_3 paste for stereolithography 3D printing applications. *J. Alloys Compd.* **2020**, *828*, 154347.
4. Geisler, E.; Lecompère, M.; Soppera, O. 3D printing of optical materials by processes based on photopolymerization: Materials, technologies, and recent advances. *Photonics Res.* **2022**, *10*, 1344–1360.
5. Kalsoom, U.; Nesterenko, P.N.; Paull, B. Recent developments in 3D printable composite. *RSC Adv.* **2016**, *6*, 60355.
6. Zakeri, S.; Vippola, M.; Levänen, E. A comprehensive review of the photopolymerization of ceramic resins used in stereolithography. *Addit. Manuf.* **2020**, *35*, 101177.

7. Shuai, X.; Zeng, Y.; Li, P.; Chen, J. Fabrication of fine and complex lattice structure Al_2O_3 ceramic by digital light processing 3D printing technology. *Ceramics* **2020**, *55*, 6771–6782.
8. Bove, A.; Calignano, F.; Galati, M.; Iuliano, L. Protopolymerization of ceramic resins by stereolithography process: A review. *Appl. Sci.* **2022**, *12*, 3591.
9. Liu, H.; Mo, J. Study on nanosilicaa reinforced stereolithography resins. *J. Reinf. Plast. Compos.* **2010**, *29*, 909–920.
10. Sprenger, S. Nanosilica-toughened epoxy resins. *Polymers* **2020**, *12*, 1777.
11. Hafkamp, T.; van Baars, G.; de Jager, B.; Etman, P. A feasibility study on process monitoring and control in vat photopolymerization of ceramics. *Mechatronics* **2018**, *56*, 220–241.
12. Ryu, K.; Kim, J.; Choi, J.; Kim, U. The 3D Printing Behavior of Photocurable Ceramic/Polymer Composite Slurries Prepared with Different Particle Sizes. *Nanomaterials* **2022**, *12*, 2631.
13. Griffith, M.L.; Halloran, J.W. Scattering of ultraviolet radiation in turbid suspensions. *Appl. Phys.* **1997**, *81*, 2538–2546.
14. Chartier, T.; Chaput, C.; Doreau, F.; Loiseau, M. Stereolithography of structural complex ceramic parts. *Mater. Sci.* **2002**, *37*, 3141–3147.
15. Licciulli, A.; Corcione, C.E.; Greco, A.; Amicarelli, V.; Maffezzoli, A. Laser stereolithography of ZrO_2 toughened Al_2O_3. *J. Eur. Ceram. Soc.* **2005**, *25*, 1581–1589.
16. Wu, X.; Lian, Q.; Li, D.; He, X.; Meng, J.; Liu, X.; Jin, Z. Influence of boundary masks on dimensions and surface roughness using segmented exposure in ceramic 3D printing. *Ceram. Int.* **2019**, *45*, 3687–3697.
17. Liu, Y.; Zhan, L.; Wen, L.; Cheng, L.; He, Y.; Xu, B.; Wu, Q.; Liu, S. Effects of particle size and color on photocuring performance of Si_3N_4 ceramic slurry by stereolithography. *Eur. Ceram. Soc.* **2021**, *41*, 2386–2394.
18. Zhang, K.; Xie, C.; Wang, G.; He, R.; Ding, G.; Wang, M.; Dai, D.; Fang, D. High solid loading, low viscosity photosensitive Al_2O_3 slurry for stereolithography based additive manufacturing. *Ceram. Int.* **2019**, *45*, 203–208.
19. Azarmi, F.; Amiri, A. Microstructural evolution during fabrication of alumina via laser stereolithography technique. *Ceram. Int.* **2019**, *45*, 271–278.
20. Zheng, T.; Wang, W.; Sun, J.; Liu, J.; Bai, J. Development and evaluation of Al_2O_3–ZrO_2 composite processed by digital light 3D printing. *Ceram. Int.* **2020**, *46*, 8682–8688.
21. Xing, H.; Zou, B.; Lai, Q.; Huang, X.; Chen, Q.; Fu, X.; Shi, Z. Preparation and characterization of UV curable Al2O3 suspensions applying for stereolithography 3D printing ceramic microcomponent. *Powder Technol.* **2018**, *338*, 153–161.
22. Quan, H.; Zhang, T.; Xu, H.; Luo, S.; Nie, J.; Zhu, X. Photo-curing 3D printing technique and its challenges. *Bioact. Mater.* **2020**, *5*, 110–115.
23. Song, S.; Park, M.S.; Lee, J.W.; Yun, J.S. A Study on the Rheological and Mechanical Properties of Photo-Curable Ceramic/Polymer Composites with Different Silane Coupling Agents for SLA 3D Printing Technology. *Nanomaterials* **2018**, *8*, 93.